Why are effective potentials 'soft'?

2004 J. Phys.: Condens. Matter 16 7331

(http://iopscience.iop.org/0953-8984/16/41/014)

INSTITUTE OF PHYSICS PUBLISHING JOURNAL OF PHYSICS: CONDENSED MATTER

J. Phys.: Condens. Matter **16** (2004) 7331–7352 PII: S0953-8984(04)83762-7

Why are effective potentials 'soft'?

Sabine H L Klapp[1], **Dennis J Diestler**[2] **and Martin Schoen**

Stranski-Laboratorium für Physikalische und Theoretische Chemie, Sekretariat TC7, Technische Universität Berlin, Straße des 17 Juni 124, D-10623 Berlin, Germany

E-mail: sabine.klapp@fluids.tu-berlin.de, ddiestler1@unl.edu and martin.schoen@fluids.tu-berlin.de

Received 21 July 2004, in final form 24 August 2004
Published 1 October 2004
Online at stacks.iop.org/JPhysCM/16/7331
doi:10.1088/0953-8984/16/41/014

Abstract

This paper is concerned with effective potentials $\mathcal{W}_1(R)$ between interacting supramolecular particles separated by a distance R. We focus on the question of why these potentials are typically 'soft', i.e., remain finite for $R \to 0$ and vary more weakly with R than the underlying interatomic interaction potentials. On the basis of a general expression linking $\mathcal{W}_1(R)$ to the free energy $\mathcal{F}$ of the supramolecular system we investigate the origin of the apparent 'softness' of $\mathcal{W}_1(R)$ by considering a number of special model systems, starting with an atom and a diatomic molecule. This simple model already yields a $\mathcal{W}_1(R)$ that is finite at $R = 0$, but $\mathcal{W}_1(R)$ does not exhibit the slowly varying character typical of effective potentials for realistic systems. We then show that the larger length scale is recovered when one introduces both many-body interactions and thermal fluctuations within the framework of a 'toy model', that is disc-shaped supramolecular units composed of thermalized configurations of Lennard-Jones atoms. In this case, $\mathcal{W}_1(R)$ varies so slowly that it can be parametrized by estimating the free energy change associated with the overlap of the discs. The resulting overlap approximation to $\mathcal{W}_1(R)$ behaves qualitatively like ad hoc effective potentials used in mesoscale simulations, such as dissipative particle dynamics. Indeed, on the basis of Monte Carlo simulations and a solution of hypernetted chain integral equations, we find that fluids interacting via DPD and overlap potentials have very similar structural and thermophysical properties. Moreover, the 'overlap' fluid (like other 'effective' fluids) turns out to be so 'soft' that its properties, particularly at high densities, can be very well estimated by a mean-field treatment.

[1] Author to whom any correspondence should be addressed.

[2] Permanent address: Department of Agronomy and Horticulture, University of Nebraska-Lincoln, Lincoln, NE 68583-0915, USA.

1. Introduction

In recent years theoretical treatments and computer simulations of macromolecular and supramolecular systems have attracted growing interest, stimulated partly by the experimental progress in preparing functionalized nanostructured fluids [1]. From a theoretical point of view, the challenge in investigating such systems consists of dealing with a huge number of microscopic degrees of freedom corresponding to the macromolecules themselves and to the solvent (if present). In fact, fully atomistic simulations for such systems are usually incapable of accessing length and timescales characterizing the phenomena of interest, which typically take place on the mesoscale. An example is the self-assembly of surfactant solutions into micelles, a process occurring on scales of length and time of about 100 nm and 1 μs, respectively [2]. For that reason, several mesoscopic simulation techniques have been established which are based on *coarse-grained* models involving only those degrees of freedom that one is actually interested in (e.g., the centres of mass (com's)), while less relevant internal degrees of freedom are integrated out. The remaining 'particles' then interact via *effective potentials* reflecting the internal configurations only implicitly.

A specific example of an effective potential is one that has been employed within the context of dissipative particle dynamics (DPD) [3–6]. It assumes the form [6] $\mathcal{W}^{\mathrm{DPD}}(R) = a(1 - R/D)^2$ where R is the separation between the com's of a pair of 'beads' representing clusters of atoms of a macromolecule or a solvent, D is the mean diameter of a bead, and a is a positive constant. Subsequently in this work we refer to the fluid consisting of particles that interact pairwise according to $\mathcal{W}^{\mathrm{DPD}}(R)$ as a 'DPD' fluid. The specific functional form of $\mathcal{W}^{\mathrm{DPD}}$ is an ansatz and lacks, in fact, any fundamental (microscopic) basis. It is so devised as to possess the main features that have been identified as essential for a proper coarse-grained description of macromolecular systems [7, 8]: $\mathcal{W}^{\mathrm{DPD}}(R)$ varies much more slowly than a typical interatomic pair potential, say a Lennard-Jones one; its range is approximately the diameter of the bead; it remains finite as $R \to 0$, which indicates that the beads can overlap completely. The motivation for this paper is a search for the microscopic basis of these features of effective potentials. We are interested in identifying the ingredients causing 'softness' and such simple functional forms as $\mathcal{W}^{\mathrm{DPD}}(R)$, rather than in constructing effective potentials for specific systems.

Explicit expressions for $\mathcal{W}(R)$ have already been derived for linear polymer chains [9–13], star polymers [14], and spherical dendrimers [15, 16]. These derivations are based on a precise statistical mechanical definition of $\mathcal{W}(R)$ involving an integration of the Boltzmann factor over the irrelevant degrees of freedom [7, 8]. A similar procedure has been used for the derivation of effective potentials between large colloidal particles in solution [17]. A prominent result of such coarse-graining procedures is the Gaussian potential for linear polymers, which has the characteristics of a soft potential described above [10]. In comparison to the case for those previous studies, the systems considered in the present work are much less realistic, but have the advantage that the effect of 'ingredients' such as size and internal structure of the molecules on the resulting effective potential can be investigated more readily.

Section 2.1 of the paper is given over to a derivation of the general expression for the effective potential energy of a system of mesoscopic particles, following essentially the lines presented in [7, 8]. The general expression is then specialized in section 2.2 to the situation where only pair interactions are significant. In sections 2.3 and 2.4 we give explicit expressions for the effective potential for a hierarchy of bimolecular systems of increasing complexity. The simplest system investigated consists of an atom plus a diatomic molecule, while the most complex case involves two 'glassy discs' with liquid-like, yet frozen internal configurations of atoms. Inspired by the disordered internal structure of the discs, we also present in section 2.5 a

simple parametrization of the effective interaction in terms of the free energy change associated with the *overlap* of the discs.

Numerical results are presented in section 3. On the basis of the model systems introduced in section 2 we systematically examine the effects of size, dimensionality, nature of microscopic interactions, and internal structure on the resulting effective potential (sections 3.1–3.3). The characteristic 'softness' of *mesoscopic* effective potentials is recovered only for the 'glassy discs'. Moreover, we show that the effective potential can be parametrized by the overlap approximation derived in section 2.5. This motivates us to examine in section 3.4 thermophysical properties of a three-dimensional 'overlap' fluid, that is a system of spherical particles interacting via the overlap pair potentials. The goal is to show that the 'overlap' fluid has 'soft' features similar to those of other fluids interacting via effective potentials [7] such as the 'Gaussian' and 'DPD' fluids. To this end, we investigate properties such as the density dependence of the pair correlation function and the pressure, employing both (quasi-exact) Monte Carlo (MC) simulations and integral equations in the hypernetted chain (HNC) approximation. It turns out that the MC and HNC approaches yield nearly identical results, especially at high densities where thermophysical properties of the 'overlap' fluid become mean-field-like. Our conclusions are summarized in section 4.

2. Theory of the effective potential

2.1. The effective many-body potential for a polyatomic molecular system

For the sake of concreteness we consider a polyatomic molecular system and seek an effective potential that governs the com motion of the molecules. The original Hamiltonian can be written as

$$H = \sum_a \sum_{i=1}^{N_a} \left[\frac{\boldsymbol{P}_i^a \cdot \boldsymbol{P}_i^a}{2M_a} + h_i^a \right] + U \tag{2.1}$$

where a labels the species and N_a is the number of molecules of that species, which has molecular mass M_a. Momentum $\boldsymbol{P}_i^a$ is conjugate to the com position $\boldsymbol{R}_i^a$ of the ith molecule of species a; the 'internal' Hamiltonian h_i^a pertains to the $3(n_a - 1)$ internal (i.e., rotational, vibrational) degrees of freedom, where n_a is the number of atoms in molecules of species a; U stands for the intermolecular interactions.

We assume that U can be decomposed into pair interactions as

$$U = \sum_a \sum_b \sum_{i=1}^{N_a} \sum_{j=1}^{N_b} U_{ij}^{ab} \tag{2.2}$$

where U_{ij}^{ab} signifies the interaction between molecule i of species a and molecule j of species b, and

$$U_{ij}^{ab} = \sum_{k=1}^{n_a} \sum_{l=1}^{n_b} \varphi(r_{ikjl}^{ab}) \tag{2.3}$$

where φ is the interaction between atom k of molecule i (species a) and atom l of molecule j (species b). The potential φ depends only on the interatomic distance $r_{ikjl}^{ab} = |\boldsymbol{r}_{ik}^a - \boldsymbol{r}_{jl}^b|$, where $\boldsymbol{r}_{ik}^a$ and $\boldsymbol{r}_{jl}^b$ are the absolute positions of the two atoms involved. Specifically, we take the interatomic potentials to be represented by a generalized Lennard-Jones (LJ) (12, 6) form

$$\varphi(r) = 4\epsilon \left[\left(\frac{\sigma}{r} \right)^{12} - \lambda \left(\frac{\sigma}{r} \right)^{6} \right] \tag{2.4}$$

where ϵ sets the energy scale and σ denotes the 'diameter' of an atom; the dimensionless parameter $0 \leqslant \lambda \leqslant 1$ is used to switch between the conventional LJ (12, 6) potential ($\lambda = 1$) and a soft-spheres potential with purely repulsive intermolecular interactions ($\lambda = 0$).

For the following derivations it is important to note that, independently of the actual choice of φ, the interatomic separations r_{ijkl}^{ab} determining the interaction energy U_{ij}^{ab} are implicit functions both of the separation between the com's of i and j, $R_{ij}^{ab} = |\boldsymbol{R}_i^a - \boldsymbol{R}_j^b|$, and of the internal coordinates (e.g., relative positions, Euler angles, or normal-mode coordinates) $\boldsymbol{q}_{ik}^a$ ($k = 1, \ldots, n_a - 1$) and $\boldsymbol{q}_{jl}^b$ ($l = 1, \ldots, n_b - 1$) of the molecules i and j. Using then the com's and the internal coordinates (instead of the absolute atomic positions) as variables, we can express the classical canonical partition function as

$$Q = \frac{1}{\prod_a N_a! \theta_a^{N_a} h^{3n_a N_a}} \int \mathrm{d}\boldsymbol{R} \int \mathrm{d}\boldsymbol{P} \int \mathrm{d}\boldsymbol{q} \int \mathrm{d}\boldsymbol{p} \exp(-\beta H) \tag{2.5}$$

where θ_a is the symmetry number of species a, h is Planck's constant, $\beta \equiv 1/k_\mathrm{B}T$, k_B is Boltzmann's constant, and T is the absolute temperature. Note the severely compacted notation in (2.5):

$$\mathrm{d}\boldsymbol{R} = \prod_a \prod_{i=1}^{N_a} \mathrm{d}\boldsymbol{R}_i^a \tag{2.6}$$

$$\mathrm{d}\boldsymbol{q} = \prod_a \prod_{i=1}^{N_a} \prod_{k=1}^{3(n_a-1)} \mathrm{d}q_{ik}^a. \tag{2.7}$$

An analogous notation is used in (2.5) for the integrations over the internal and com momenta $\boldsymbol{p}_{ik}^a$ and $\boldsymbol{P}_i^a$, respectively. Integrating out the latter, we can rewrite (2.5) as

$$Q = \frac{1}{\prod_a N_a! \Lambda_a^{3N_a}} \int \mathrm{d}\boldsymbol{R} \exp[-\beta \mathcal{W}(\boldsymbol{R})] \tag{2.8}$$

where $\Lambda_a \equiv (h^2/2\pi M_a k_\mathrm{B} T)^{1/2}$ is the thermal de Broglie wavelength and $\mathcal{W}$ is the effective potential energy, given by

$$\mathcal{W}(\boldsymbol{R}) \equiv -k_\mathrm{B}T \ln \left[\frac{1}{\prod_a \theta_a^{N_a} h^{3(n_a-1)N_a}} \int \mathrm{d}\boldsymbol{q} \int \mathrm{d}\boldsymbol{p} \exp\left(-\beta \sum_a \sum_{i=1}^{N_a} h_i^a \right) \exp(-\beta U) \right]. \tag{2.9}$$

The argument of the logarithm in (2.9) may be recognized as the canonical partition function of the system with the com's of the molecules fixed in the configuration $\boldsymbol{R}$. Thus, $\mathcal{W}$ is the effective Helmholtz potential of the system 'frozen' in that configuration. In the following we make use of the fact that the effective potential defined by (2.9) depends on the actual configuration $\boldsymbol{R}$ only through the interaction part of the Boltzmann factor $\exp(-\beta U)$. Therefore, it is convenient to recast $\mathcal{W}$ in the (still exact) form

$$\mathcal{W}(\boldsymbol{R}) = -k_\mathrm{B}T \ln \left[Q_0 \left\langle \exp\left(-\beta U\right) \right\rangle_0 \right] \tag{2.10}$$

where

$$Q_0 \equiv \frac{1}{\prod_a \theta_a^{N_a} h^{3(n_a-1)N_a}} \int \mathrm{d}\boldsymbol{q} \int \mathrm{d}\boldsymbol{p} \exp\left(-\beta \sum_a \sum_{i=1}^{N_a} h_i^a \right) \tag{2.11}$$

is the partition function for the 'non-interacting' system, that is the system with vanishing interatomic interactions U (see (2.2) and (2.3)), and the angular brackets $\langle \cdots \rangle_0$ stand for an ensemble average over the states of this non-interacting system. Explicitly, one has

$$\langle X \rangle_0 = \frac{\int \mathrm{d}\boldsymbol{q} \int \mathrm{d}\boldsymbol{p} \exp(-\beta \sum_a \sum_{i=1}^{N_a} h_i^a) X(\boldsymbol{q}, \boldsymbol{p})}{\int \mathrm{d}\boldsymbol{q} \int \mathrm{d}\boldsymbol{p} \exp(-\beta \sum_a \sum_{i=1}^{N_a} h_i^a)}. \tag{2.12}$$

Note that if $X = X(\boldsymbol{q})$ (i.e., if X is independent of the momenta), as is the case of interest here, where $X = \exp(-\beta U)$, then the integration on $\boldsymbol{p}$ can be carried out to give

$$\langle X\rangle_0 = \frac{\int \mathrm{d}\boldsymbol{q}\,\gamma(\boldsymbol{q})\exp(-\beta\sum_a\sum_{i=1}^{N_a} v_i^a)X(\boldsymbol{q})}{\int \mathrm{d}\boldsymbol{q}\,\gamma(\boldsymbol{q})\exp(-\beta\sum_a\sum_{i=1}^{N_a} v_i^a)} \tag{2.13}$$

where v_i^a is the internal potential energy of molecule i of species a and the factor $\gamma(\boldsymbol{q})$ arises from terms in the internal kinetic energies that contain factors depending on the (generalized) internal coordinates.

Equation (2.10) can be rewritten as

$$\mathcal{W}(\boldsymbol{R}) = -k_\mathrm{B}T\ln Q_0 - k_\mathrm{B}T\ln\langle\exp(-\beta U)\rangle_0 \tag{2.14}$$

where the first term is the free energy of the non-interacting system and the second term is the 'correction' to the free energy due to the interactions among molecules frozen in configuration $\boldsymbol{R}$. Since Q_0 does not depend on $\boldsymbol{R}$, the non-interacting term in (2.14) has no influence on the motion of the com's, although it does contribute to the thermodynamic properties, which are expressible as derivatives of the Helmholtz potential

$$\mathcal{F} = -k_\mathrm{B}T\ln Q \tag{2.15}$$

with respect to the controlled state variables (i.e., T, $\{N_a\}$, and volume V). Henceforth we focus on the correction

$$\mathcal{W}_1(\boldsymbol{R}) \equiv -k_\mathrm{B}T\ln\langle\exp(-\beta U)\rangle_0. \tag{2.16}$$

2.2. The effective pair potential

Inspecting the rhs of (2.16) we observe that the effective potential $\mathcal{W}_1(\boldsymbol{R})$ cannot be expressed simply as a sum of pair interactions, despite the (original) potential energy (see (2.2)) being assumed to be so expressible. The reason is the appearance of many-body correlations in the ensemble average $\langle\exp(-\beta U)\rangle_0$, which makes it impossible to factor the latter. Nevertheless, to realize some progress toward a pair description of $\mathcal{W}_1(\boldsymbol{R})$, we suppose the density to be low and express the Boltzmann factor as a Mayer cluster expansion (see, e.g., [18])

$$\exp(-\beta U) = \prod_{ab}\prod_{1\leqslant i\leqslant N_a,\,1\leqslant j\leqslant N_b}\left(1+f_{ij}^{ab}\right) \tag{2.17}$$

$$\simeq 1 + \sum_a\sum_b\sum_{i=1}^{N_a}\sum_{j\neq i}^{N_b} f_{ij}^{ab} \tag{2.18}$$

where

$$f_{ij}^{ab} = \exp(-\beta U_{ij}^{ab}) - 1 \tag{2.19}$$

is the Mayer f-function and we have neglected three-body and higher-order terms on the rhs of (2.18). Substituting this approximation for $\exp(-\beta U)$ into (2.16), we obtain

$$\mathcal{W}_1(\boldsymbol{R}) \simeq -k_\mathrm{B}T\ln\left\{1+\sum_a\sum_b\sum_{i=1}^{N_a}\sum_{j\neq i}^{N_b}\left[\frac{Z_{ij}^{ab}\left(\boldsymbol{R}_{ij}^{ab}\right)}{Z_{ij,0}^{ab}} - 1\right]\right\}. \tag{2.20}$$

In (2.20) the pair configuration integrals are defined by

$$Z_{ij}^{ab}(\boldsymbol{R}_{ij}^{ab}) \equiv \int \mathrm{d}\boldsymbol{q}_i^a\,\gamma_i^a\int \mathrm{d}\boldsymbol{q}_j^b\,\gamma_j^b\exp[-\beta(v_i^a+v_j^b)]\exp(-\beta U_{ij}^{ab}) \tag{2.21}$$

$$Z_{ij,0}^{ab} \equiv \int \mathrm{d}\boldsymbol{q}_i^a\,\gamma_i^a\exp(-\beta v_i^a)\int \mathrm{d}\boldsymbol{q}_j^b\,\gamma_j^b\exp(-\beta v_j^b) \tag{2.22}$$

where $\mathrm{d}\boldsymbol{q}_i^a = \prod_{k=1}^{3(n_a-1)} \mathrm{d}q_{ik}^a$ and we have used the factorizability of the function $\gamma(\boldsymbol{q})$ appearing in (2.13), that is

$$\gamma(\boldsymbol{q}) = \prod_a \prod_{i=1}^{N_a} \gamma_i^a(\boldsymbol{q}_{ik}^a). \tag{2.23}$$

This is in turn due to the separability of the internal kinetic energies.

Note that, in spite of the truncation of the cluster expansion of the Boltzmann factor after the two-body term (see (2.18)), the resulting effective potential $\mathcal{W}_1(\boldsymbol{R})$ is still *not* a true pair potential because of the appearance of the logarithm in (2.20). In fact, a true effective *two-body* potential only results from (2.20) under the additional restriction that the system contains just *two* polyatomic molecules. In that case, we have from (2.20)

$$\mathcal{W}_1(\boldsymbol{R}) = -k_\mathrm{B}T \ln\left[\frac{Z^{ab}(\boldsymbol{R})}{Z_0^{ab}}\right] \tag{2.24}$$

where

$$Z^{ab}(\boldsymbol{R}) = \int \mathrm{d}\boldsymbol{q}^a\, \gamma^a \int \mathrm{d}\boldsymbol{q}^b\, \gamma^b \exp[-\beta(v^a + v^b)] \exp(-\beta U^{ab}) \tag{2.25}$$

and

$$Z_0^{ab} = \int \mathrm{d}\boldsymbol{q}^a\, \gamma^a \exp(-\beta v^a) \int \mathrm{d}\boldsymbol{q}^b\, \gamma^a \exp(-\beta v^b). \tag{2.26}$$

Note that the indices i and j that label particular molecules of species a and b in the general formulae (2.20)–(2.22) have disappeared since only one molecule of each species is present. The effective potential $\mathcal{W}_1$ thus reduces to a true two-body potential.

To evaluate $\mathcal{W}_1$ in practice we must compute the internal configuration integral $Z^{ab}(\boldsymbol{R})$ (see (2.25)) numerically. For that purpose we need not only to specify the internal potential energies v^a and v^b, but also to express the interatomic distances r_{kl}^{ab}, on which U^{ab} depends through (2.3), as functions of the com coordinates, $\boldsymbol{R}^a$ and $\boldsymbol{R}^b$, and internal coordinates $\boldsymbol{q}_k^a$ and $\boldsymbol{q}_l^b$. In the following the internal coordinates are chosen as vectors $\boldsymbol{\rho}_k^a$ ($\boldsymbol{\rho}_l^b$) describing the position of atom k (l) with respect to the com of molecule a (b). This implies

$$r_{kl}^{ab} = |\boldsymbol{r}_k^a - \boldsymbol{r}_l^b| = |\boldsymbol{R}^a + \boldsymbol{\rho}_k^a - \boldsymbol{R}^b - \boldsymbol{\rho}_l^b| = |\boldsymbol{R}^{ab} + \boldsymbol{\rho}_k^a - \boldsymbol{\rho}_l^b|. \tag{2.27}$$

2.3. The effective interaction between an atom and a diatomic molecule in two and three dimensions

Consider now the simplest system suitable for the introduction of an effective potential: an atom interacting with a diatomic molecule. In this case, where $n_a = 1$ and $n_b = 2$, the atom a has no internal degrees of freedom. The integral on $\boldsymbol{q}^a$ therefore disappears from the formal expressions in (2.25) and (2.26) and $\boldsymbol{\rho}_1^a = \boldsymbol{0}$ in (2.27). Moreover, we can, for convenience, take the com of the diatomic to lie at the origin (i.e., $\boldsymbol{R}^b = \boldsymbol{0}$, $\boldsymbol{R}^{ab} = \boldsymbol{R}^a = \boldsymbol{R}$). The internal coordinates of the diatomic molecule's atoms can be expressed

$$\boldsymbol{\rho}_1^b = \frac{m_2\boldsymbol{r}}{m} \tag{2.28}$$

$$\boldsymbol{\rho}_2^b = -\frac{m_1\boldsymbol{r}}{m} \tag{2.29}$$

where $\boldsymbol{r} = \boldsymbol{r}_1^b - \boldsymbol{r}_2^b$, $m = m_1 + m_2$, and m_i denotes the mass of atom i ($i = 1, 2$). Substituting these latter relations into (2.27), we obtain

$$r_{11}^{ab} = |\boldsymbol{R} - \boldsymbol{\rho}_1^b| = \left[R^2 - \frac{2m_2}{m} Rr\cos\theta + \left(\frac{m_2}{m}\right)^2 r^2\right]^{1/2} \tag{2.30}$$

$$r_{12}^{ab} = \left|\boldsymbol{R} - \boldsymbol{\rho}_2^b\right| = \left[R^2 + \frac{2m_1}{m} Rr\cos\theta + \left(\frac{m_1}{m}\right)^2 r^2\right]^{1/2} \tag{2.31}$$

where θ denotes the angle between $\boldsymbol{R}$ and $\boldsymbol{r}$.

We assume that the internal potential energy of the diatomic molecule is given by

$$v^b(r) = v^b(r_e) + \tfrac{1}{2}\kappa(r - r_e)^2 \tag{2.32}$$

where r_e is the equilibrium bond length and κ is the force constant. Since r_{kl}^{ab} depends only on the magnitude of $\boldsymbol{R}$, for convenience we take the atom on the positive z-axis and utilize spherical polar coordinates to describe the internal motion of the diatomic molecule. From the general expressions in (2.25) and (2.26) we obtain

$$Z^{ab}(R) = \int_0^{2\pi} \mathrm{d}\phi \int_{-1}^{1} \mathrm{d}x \int_0^{\infty} \mathrm{d}r\, r^2 \exp\left\{-\beta\left[v^b(r_e) + \frac{\kappa}{2}(r - r_e)^2\right]\right\} \times \exp\{-\beta[\varphi(r_{11}^{ab}) + \varphi(r_{12}^{ab})]\} \tag{2.33}$$

$$Z_0^{ab} = 4\pi \int_0^{\infty} \mathrm{d}r\, r^2 \exp\left\{-\beta\left[v^b(r_e) + \frac{\kappa}{2}(r - r_e)^2\right]\right\} \tag{2.34}$$

where $x = \cos\theta$, θ is the polar angle, ϕ is the azimuthal angle, and the arguments of the interatomic pair potentials φ depend implicitly on R, r, and x through (2.30) and (2.31). Note that since the interatomic separations r_{kl}^{ab} depend only on the magnitude of the com separation vector $\boldsymbol{R}$, the same holds for the pair configuration integral $Z^{ab}(R)$. From (2.33) and (2.34) we then obtain the crucial ratio

$$\frac{Z^{ab}(R)}{Z_0^{ab}} = \frac{1}{2}\int_0^{\infty} \mathrm{d}r\, r^2 P_{3D}(r) \int_{-1}^{1} \mathrm{d}x\, \exp\{-\beta[\varphi(r_{11}^{ab}) + \varphi(r_{12}^{ab})]\} \tag{2.35}$$

which determines $\mathcal{W}_1(R)$ through (2.24). The bond-length distribution function $P_{3D}(r)$ is defined by

$$P_{3D} = \frac{\exp[-\beta\kappa(r - r_e)^2/2]}{\int_0^{\infty} \mathrm{d}r\, r^2 \exp[-\beta\kappa(r - r_e)^2/2]}. \tag{2.36}$$

In the case where the diatomic molecule is rigid (i.e., r is fixed at $r = r_e$), the only internal coordinates of the diatomic molecule are the angles θ and ϕ. Equations (2.33) and (2.34) then reduce to

$$Z^{ab}(R) = \int_0^{2\pi} \mathrm{d}\phi \int_{-1}^{1} \mathrm{d}x\, \exp[-\beta v^b(r_e)] \exp\{-\beta[\varphi(r_{11}^{ab}) + \varphi(r_{12}^{ab})]\} \tag{2.37}$$

$$Z_0^{ab} = 4\pi \exp[-\beta v^b(r_e)] \tag{2.38}$$

and we have therefore

$$\frac{Z^{ab}(R)}{Z_0^{ab}} = \frac{1}{2}\int_{-1}^{1} \mathrm{d}x\, \exp\{-\beta[\varphi(r_{11}^{ab}) + \varphi(r_{12}^{ab})]\}. \tag{2.39}$$

Note that this latter expression may also be reached directly from (2.35) through the identity

$$\lim_{\kappa\to\infty} P_{3D}(r) = \frac{\delta(r - r_e)}{r_e^2} \tag{2.40}$$

where δ stands for Dirac's delta function and the limit corresponds to the infinitely stiff (i.e., rigid) bond.

The explicit formulae (2.33)–(2.39) refer to three-dimensional (3D) systems. If, on the other hand, the system is confined to a plane, then (2.35) is replaced by

$$\frac{Z^{ab}(R)}{Z_0^{ab}} = \frac{1}{2\pi}\int_0^{\infty} \mathrm{d}r\, r P_{2D}(r) \int_0^{2\pi} \mathrm{d}\theta\, \exp\{-\beta[\varphi(r_{11}^{ab}) + \varphi(r_{12}^{ab})]\} \tag{2.41}$$

where θ is now the angle between $\boldsymbol{r}$ and the positive x-axis, along which lies $\boldsymbol{R}$, and r_{11}^{ab} and r_{12}^{ab} are still given by (2.30) and (2.31). Also, the 2D analogue of the bond-length distribution is given by

$$P_{2D} = \frac{\exp[-\beta\kappa(r - r_e)^2/2]}{\int_0^\infty \mathrm{d}r\, r \exp[-\beta\kappa(r - r_e)^2/2]}. \tag{2.42}$$

Finally, in the limit of a rigid diatomic molecule (i.e., for $\kappa \to \infty$), (2.41) simplifies to

$$\frac{Z^{ab}(R)}{Z_0^{ab}} = \frac{1}{2\pi}\int_0^{2\pi} \mathrm{d}\theta\, \exp\{-\beta[\varphi(r_{11}^{ab}) + \varphi(r_{12}^{ab})]\}. \tag{2.43}$$

The effective potentials $\mathcal{W}_1(R) = -k_B T \ln[Z^{ab}(R)/Z_0^{ab}]$ corresponding to the various 'atom plus diatomic molecule' systems introduced above can be easily evaluated by numerical integration of the integrals on the rhs of (2.35), (2.39), (2.41), and (2.43). Any standard integration technique can be used for this calculation [19] (we employed an extended trapezoidal rule based on cubic spline interpolation). Numerical results are presented in section 3.1.

2.4. The effective interaction between two rigid, planar polyatomic molecules

In addition to the simple, well-defined model systems discussed in section 2.3, where the effective potential can be evaluated nearly analytically, we will also consider below (see section 3.3) effective interactions between two larger, planar molecules a and b with highly disordered, yet frozen internal configurations specified by the atomic positions $\boldsymbol{r}_k^a$ ($k = 1, \ldots, n_a$) and $\boldsymbol{r}_l^b$ ($l = 1, \ldots, n_b$). Starting from these configurations, the effective interaction $\mathcal{W}_1(R)$ is calculated from the general formulae (2.24), (2.25), and (2.26) as follows.

We first determine the com positions $\boldsymbol{R}^a$ and $\boldsymbol{R}^b$ and take the direction of the vector $\boldsymbol{R} = \boldsymbol{R}^a - \boldsymbol{R}^b$ to coincide with the x-axis of our two-dimensional coordinate system. Next, we calculate the relative atomic positions $\boldsymbol{\rho}_k^a = \boldsymbol{r}_k^a - \boldsymbol{R}^a$ and $\boldsymbol{\rho}_l^b = \boldsymbol{r}_l^b - \boldsymbol{R}^b$, the magnitudes of these vectors, that is $\rho_k^a = |\boldsymbol{\rho}_k^a|$ and $\rho_l^b = |\boldsymbol{\rho}_l^b|$, and, on the basis of these quantities, the angles $\theta_k^a = \cos^{-1}(\rho_{k,x}^a/\rho_k^a)$ and $\theta_l^b = \cos^{-1}(\rho_{l,x}^b/\rho_l^b)$ between $\boldsymbol{\rho}_k^a$ ($\boldsymbol{\rho}_l^b$) and the x-axis ($\rho_{k,x}^a$ and $\rho_{l,x}^b$ are the x-components of the relative position vectors). The interatomic separation then follows from (2.27) as

$$r_{kl}^{ab} = [R^2 + (\rho_k^a)^2 + (\rho_l^b)^2 + 2R\rho_k^a \cos\theta_k^a - 2R\rho_l^b \cos\theta_l^b - 2\rho_k^a \rho_l^b \cos(\theta_k^a - \theta_l^b)]^{-\frac{1}{2}}. \tag{2.44}$$

Note that quantities ρ_k^a (ρ_l^b) and θ_k^a (θ_l^b) are all fixed for any given internal structure of the two rigid polyatomic molecules. Therefore, at fixed com separation R, the only transformations determining the effective interaction between the polyatomic molecules are *rotations* relative to each other, and these can be described by the angles of just two (arbitrary) 'reference' atoms within each polyatomic molecule, say θ_1^a and θ_1^b. We thus formally replace the angles appearing in (2.44) by $\theta_k^a = \theta_1^a + \Delta\theta_k^a$ and $\theta_l^b = \theta_1^b + \Delta\theta_l^b$ where θ_1^a and θ_1^b are the variables, and $\Delta\theta_k^a$ ($\Delta\theta_l^b$) are fixed for any given internal structure. The crucial ratio determining the effective potential $\mathcal{W}_1(R)$ (see (2.24)) can then be written as

$$\frac{Z^{ab}(R)}{Z_0^{ab}} = \frac{1}{(2\pi)^2}\int_0^{2\pi} \mathrm{d}\theta_1^a \int_0^{2\pi} \mathrm{d}\theta_1^b\, \exp\left\{-\beta \sum_{k=1}^{n}\sum_{l=1}^{n} \varphi(r_{kl}^{ab})\right\}. \tag{2.45}$$

Here we have set the internal potential energies appearing in (2.25) and (2.26) to zero, since we are considering rigid polyatomic molecules.

2.5. The overlap approximation to the effective potential

In order to parametrize the effective potentials between larger, highly disordered supramolecules considered in section 3.3, it will prove useful to introduce a simple approximation. This is based upon the interpretation of $\mathcal{W}(R)$ as the Helmholtz free energy of the system with the com's of the supramolecules fixed in the configuration $\boldsymbol{R}$(see the discussion below (2.9)). According to (2.10) we can express $\mathcal{W}_1(R)$ as the difference between this free energy and the free energy when the com's are fixed such that all molecules are sufficiently far apart that their interactions are negligible.

For simplicity we restrict our consideration to a system comprising a single pair of identical supramolecules and estimate this free energy difference very roughly. We assume that the particles are spheres of radius r_0 and volume $V = 4\pi r_0^3/3$. We further assume that the particles do not interact unless they overlap (i.e., unless $R < 2r_0$). If $R < 2r_0$, we approximate the free energy of the interacting system as

$$\mathcal{F}(R) \simeq V_o(R) f_o + 2[V - V_o(R)] f \tag{2.46}$$

where V_o and $2[V - V_o(R)]$ are the respective volumes of the overlapping and non-overlapping regions of the particles and f_o and f are the Helmholtz potential densities associated with these regions. If $R > 2r_0$, then

$$\mathcal{F} = 2Vf. \tag{2.47}$$

Implicit in (2.46) and (2.47) is the assumption that f and f_o are constant throughout their respective regions and independent of R. Combining (2.46) and (2.47), we obtain for the free energy difference, with which we identify $\mathcal{W}_1(R)$,

$$\begin{aligned} \mathcal{W}_1(R) &= \mathcal{F}(R) - \mathcal{F} \\ &= \Delta f V_o(R) \end{aligned} \tag{2.48}$$

where $\Delta f = f_o - 2f$.

We note in passing that the idea of the overlap volume $V_o(R)$ determining the effective potential between two molecules has also been used in other contexts, such as in the construction of the Gay–Berne potential for liquid crystal molecules [20].

The volume of the overlapping region is twice the volume of the spherical cap [21]

$$V_c = \frac{\pi h^2}{3}(3r_0 - h) \tag{2.49}$$

of height h, where the height of the cap is related to R and r_0 by

$$h = r_0 - \frac{R}{2}. \tag{2.50}$$

Substituting (2.50) into (2.49) and simplifying, we get

$$V_o(R) = \frac{4\pi r_0^3}{3}\left[1 - \frac{3}{2}\alpha(R) + \frac{1}{2}\alpha^3(R)\right] \tag{2.51}$$

where

$$\alpha(R) = \frac{R}{2r_0}. \tag{2.52}$$

For a 2D system the spheres are replaced by discs of radius r_0. A straightforward calculation paralleling the 3D one yields for the area of the overlapping region [21]

$$A_o = 2r_0^2\left\{\arccos[\alpha(R)] - \alpha(R)\sqrt{1 - \alpha^2(R)}\right\} \tag{2.53}$$

where again $\alpha(R)$ is defined in (2.52). Combining now (2.48), (2.51), (2.52), and (2.53) we get the 'overlap' potential

$$\mathcal{W}_1(R) = \begin{cases} \left.\begin{array}{ll} a_{2D}\left[\arccos\alpha - \alpha\sqrt{1-\alpha^2}\right] & 2D \\ a_{3D}\left[1 - \frac{3}{2}\alpha + \frac{1}{2}\alpha^3\right] & 3D \end{array}\right\} & 0 \leqslant \alpha \leqslant 1 \\ 0 & \alpha > 1 \end{cases} \tag{2.54}$$

where a_{2D} and a_{3D} are undetermined constants setting the energy scales in the 2D and 3D systems, respectively. In section 3.3 we employ the 2D overlap potential (2.54) as the fit function, taking a_{2D} as the parameter. Implications of the *shape* of the overlap potentials for various thermophysical properties are discussed in section 3.4.

3. Numerical results

3.1. An atom plus a diatomic molecule

The influence of bond lengths. We begin with the simplest case, namely that of an atom interacting with a rigid, homonuclear diatomic molecule ($m_1 = m_2$) in two dimensions. Setting the dimensionless temperature $k_B T/\epsilon = 1$ (where ϵ is the LJ energy unit; see (2.4) with $\lambda = 1$) we calculate the effective potential $\mathcal{W}_1(R)$ from (2.24) and (2.43) as a function of the (fixed) bond length r_e (in units of the LJ (or SS) diameter σ).

It is convenient to consider first the limit $r_e = 0$, where the diatomic molecule degenerates into a single LJ atom. As a consequence one has

$$\mathcal{W}_1(R) = 2\beta\varphi(R) \tag{3.1}$$

which follows from (2.43) and (2.24) by noting that for the degenerate case $r_{11}^{ab} = r_{12}^{ab} = R$ and therefore

$$\frac{Z^{ab}(R)}{Z_0^{ab}} = \exp[-2\beta\varphi(R)]. \tag{3.2}$$

The plot labelled $2\varphi_{LJ}(R)/\epsilon$ in figure 1(a) confirms this result. Plots in figure 1(a) also indicate that with increasing bond length r_e the minimum shifts to larger R and becomes shallower, while a second minimum at shorter com separation gradually appears (see plot for $r_e/\sigma = 1.8$ in figure 1(a)). The secondary (but only weakly pronounced) minimum corresponds to the atom located on the bond axis halfway between the two atoms of the diatomic molecule.

Another noteworthy feature of the dependence of $\mathcal{W}_1(R)$ on r_e is illustrated in figure 1(b) where we focus on intermediate (non-zero) values of the bond length ($1.5 < r_e < 1.9$). For this range of r_e the effective potential $\mathcal{W}_1(R)$, unlike the interatomic pair potential $\varphi(R)$, remains *finite* as $R \to 0$. Moreover, the strength of the repulsion decreases gradually with increasing r_e. This behaviour is intuitively reasonable, since the atom is never forced to coincide with either atom of the diatomic molecule when $r_e > 0$; it is especially significant because it agrees with the behaviour of more realistic effective potentials [7]. A prominent example is the Gaussian, which has previously been shown to describe well the effective potential for such macromolecular systems as polymer coils [7, 9, 22] and dendrimers [15, 16]. Surveying the plots in figure 1(b), one might be tempted to assume that $\mathcal{W}_1(R)$ could also be represented reasonably well by a Gaussian. We have tested this notion by computing the second and fourth central moments μ_2 and μ_4 of $\mathcal{W}_1(R)$, which for a Gaussian should satisfy the relation

$$\frac{3\mu_2^2}{\mu_4} = 1. \tag{3.3}$$

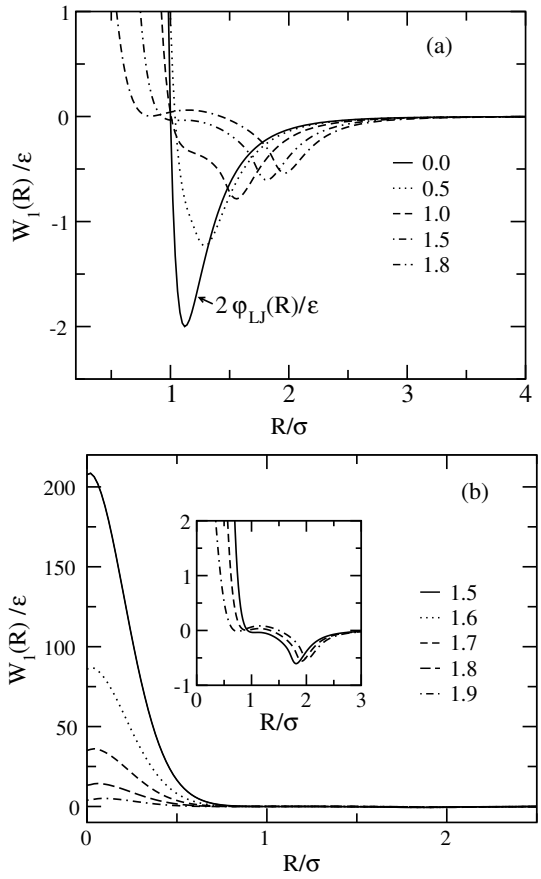

Figure 1. The effective potential for an atom interacting with a rigid homonuclear diatomic molecule in 2D via LJ interatomic potentials (see (2.4), with $\lambda = 1$) for various bond lengths r_e. Curves are labelled with values of r_e/σ.

Typical values of this ratio are always much smaller than 1 for the five curves plotted in figure 1(b), thereby reflecting the strongly non-Gaussian character of our $\mathcal{W}_1(R)$ obtained for the simple system to hand. We note in passing that increasing r_e to values of twice the LJ diameter or more causes $\mathcal{W}_1(R)$ to look rather unphysical in that it exhibits potential barriers at small but non-zero com separations and may be attractive rather than repulsive in the limit $R = 0$. These features suggest that the range of bond length over which evaluation of the effective potential is physically sensible for this model is quite limited.

The relevance of attractive tails. By setting $\lambda = 0$ in (2.4) we 'switch off' intermolecular attractions. Plots of $\mathcal{W}_1(R)$ for the 2D system of an atom plus a homonuclear diatomic molecule in figure 2(a) show that the effective potential is again 'soft' and finite even at $R = 0$ for the bond lengths considered and that the repulsion weakens with increasing r_e. Thus, the dependence of the effective potential on r_e is similar to that of the corresponding LJ system. Direct comparison of the resulting $\mathcal{W}_1(R)$'s for two model systems (that is $\lambda = 0$ (SS) versus $\lambda = 1$ (LJ)) is made in figure 2(b). The plots indicate that the SS intermolecular potential gives rise to a somewhat more strongly repulsive $\mathcal{W}_1(R)$ at short com separations because of the

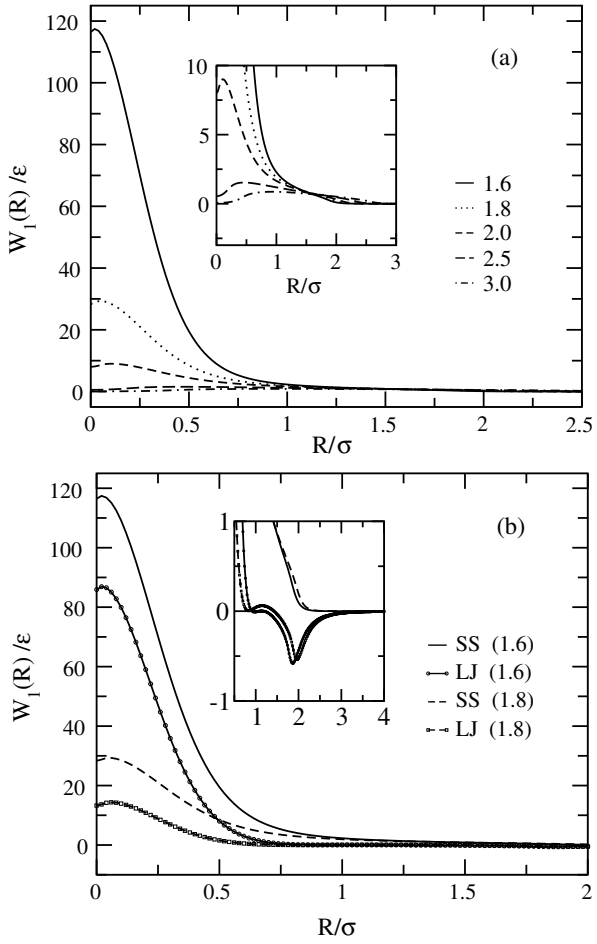

Figure 2. (a) The same as figure 1, but for soft-sphere (SS) interatomic potentials (see (2.4), with $\lambda = 0$) and bond lengths $1.6 \leqslant r_e/\sigma \leqslant 3.0$. (b) Comparison of the effective potentials based on SS and LJ interactions for $r_e/\sigma = 1.6$ and 1.8.

lack of intermolecular attraction. A further consequence of the absence of attraction, which is illustrated in the inset in figure 2(b), is that $\mathcal{W}_1(R)$ goes to zero monotonically whereas it has a minimum in the LJ case. Apart from these subtle differences, however, the $\mathcal{W}_1(R)$'s are actually quite similar in that they remain finite in the limit $R = 0$, unlike the underlying interatomic potential φ.

The influence of the spatial dimension. So far we have been considering the effective potential between an atom and a diatomic molecule in *two* dimensions. However, on the basis of (2.24) and (2.39) we may also consider 3D systems. Results obtained for an underlying LJ interatomic potential are plotted in figure 3. It is seen that dimensionality (i.e., 2D versus 3D) has only a negligible impact on $\mathcal{W}_1(R)$ as far as the repulsive part of the effective potential is concerned. On the other hand, subtle differences occurring around the minimum of $\mathcal{W}_1(R)$ can be seen in the inset in figure 3. Specifically, the range over which the effective potential is negative is somewhat wider for the 3D than for the 2D system. We speculate that this difference is due to

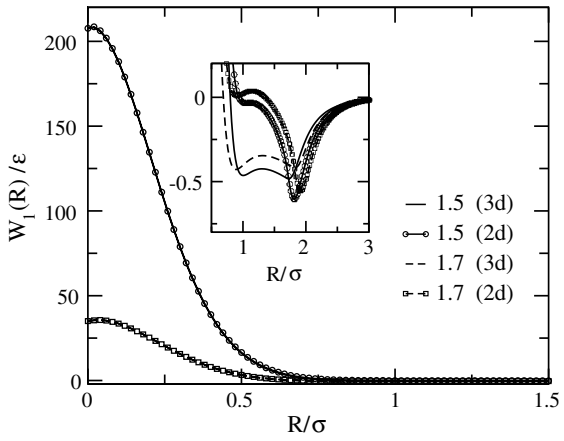

Figure 3. Comparison of effective potentials for a LJ atom–diatomic molecule system in 2D and 3D for two bond lengths $r_e/\sigma = 1.5$ and 1.7.

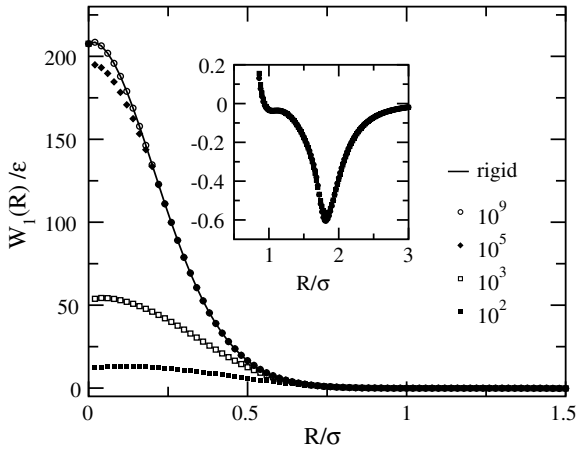

Figure 4. The influence of harmonic vibrations on the effective potential of a 2D LJ atom–diatomic molecule system (equilibrium bond length $r_e/\sigma = 1.5$) for various dimensionless force constants $10^2 \leqslant \beta\kappa\sigma^2 \leqslant 10^9$. The result for the corresponding rigid diatomic molecule is included as a reference.

what one might refer to as an entropic effect: more attractive configurations are available in the 3D system than in the 2D system.

The influence of vibrations. Finally, it is instructive to consider the influence of intermolecular vibrations on $\mathcal{W}_1(R)$. We limit the treatment to a classical harmonic oscillator (see (2.32)), for which $\mathcal{W}_1(R)$ is generated in 3D from (2.35) and (2.36) or in 2D from (2.41) and (2.42). Results are plotted in figure 4, where we set the equilibrium bond length to $r_e/\sigma = 1.5$. From figure 4 one readily concludes that bond vibrations have a profound impact on $\mathcal{W}_1(R)$. Starting from a large (dimensionless) force constant $\beta\kappa\sigma^2 = 10^9$, where $\mathcal{W}_1(R)$ is indistinguishable from the corresponding curve for the rigid diatomic molecule, the repulsive part of $\mathcal{W}_1(R)$ substantially decreases with decreasing force constant. Specifically, as $\beta\kappa\sigma^2$ decreases from 10^9 to 10^2, $\mathcal{W}_1(0)$ decreases by roughly a factor of 17.

In sharp contrast the inset in figure 4 indicates that variations in κ have little or no influence on the attractive region of $\mathcal{W}_1(R)$. The disparate impacts of bond stiffness on the repulsive and attractive regions can be rationalized as follows. On the one hand, the repulsive part of the effective potential arises from configurations in which the atom is near the com of the diatomic molecule. Hence, the less rigid the bond is, the more easily the atom can move between the diatomic molecule's atoms and consequently the smaller the repulsion is. On the other hand, the attraction comes from configurations in which R is greater than r_e and is due to the attractive tails of the interatomic LJ pair potentials. Small oscillations of the bond length about its equilibrium length r_e are expected to cause only slight variations in the attraction.

3.2. Conclusions from studying small model systems

A major conclusion from the results presented in section 3.1 is that the simplest model systems involving only small molecules already can yield 'soft' effective potentials $\mathcal{W}_1(R)$ in the sense that they remain *finite* in the limit $R \to 0$. However, a common feature of the systems investigated so far is that $\mathcal{W}_1(R)$ vanishes on a length scale that is determined more or less by the range of the underlying interatomic potential, that is the LJ (or SS) diameter σ. This is in contrast to effective potentials for true supramolecular systems where the characteristic length scale is typically determined by the supramolecular unit itself (e.g., the radius of gyration of a polymer) rather than that of its atomic constituents [7]. It seems that two significant 'ingredients' of realistic supramolecular systems are missing from the simple atom-plus-diatomic-molecule models discussed in section 3.1. These are

(a) the presence of many atoms in the supramolecules;
(b) thermal fluctuations of the atomic positions.

Simultaneous incorporation of these ingredients along the lines followed so far, where we have *explicitly* carried out the integrations over internal degrees of freedom, can be done with reasonable numerical effort only for highly specialized 'molecules', such as linear chains, and only by using idealized models (e.g., harmonic oscillators) to describe the thermal fluctuations. In the present work, however, we are interested in *general* features of effective potentials rather than in particular potentials for specific polyatomic molecule systems. This is our motivation for adopting in the following section a 'toy model', which by construction lacks specific information about the structure of the polyatomic molecules. We restrict the discussion to 2D systems. It should be noted, however, that the following calculations could be extended to 3D systems in a straightforward fashion.

3.3. The effective potential of 'glassy' discs

The 'toy model' consists of two discs of radius $r_s = 6\sigma$, where σ is again the LJ (or SS) length scale. The latter comes into play on assuming that each disc is composed of several atoms interacting with each other according to $\varphi(r)$ (see (2.4)). To obtain the spatial arrangement of the atoms we perform an MC simulation in the canonical ensemble using a square simulation cell of side length $2r_s$. From this simulation we take two thermalized configurations (at temperature $k_B T/\epsilon = 1$) and remove all atoms outside a circle of radius r_s such that for the two configurations the number densities $\overline{\rho} = N/\pi r_s^2$ are the same. The resulting configurations of atoms then form a pair of 'glassy' discs with liquid-like, yet frozen internal atomic structure. We calculate the effective potential $\mathcal{W}_1(R)$ between the discs according to (2.45). Since the results of the integration in (2.45) depend on the specific spatial arrangement of atoms forming the glassy discs, we average the results for $\mathcal{W}_1(R)$ over 12–16 statistically independent

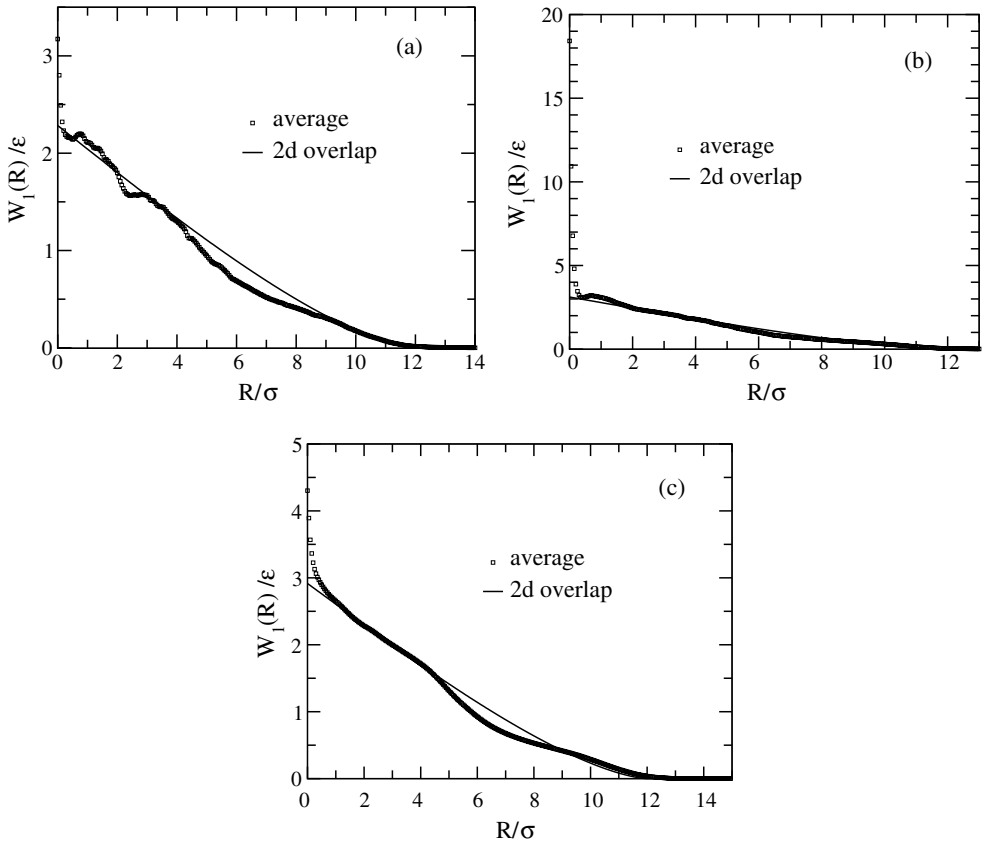

Figure 5. (a) The averaged effective potential (based on LJ interatomic potentials) between two glassy discs with diameters $2r_0 = 12\sigma$ and reduced internal density $\overline{\rho}\sigma^2 \simeq 0.13$ (solid line). Also shown are plots of the 2D overlap potential, where the parameter a_{2D} has been fixed according to the values of $\mathcal{W}_1(R)$ at $R/\sigma = 3$. (b) The same as (a) but for $\overline{\rho}\sigma^3 \simeq 0.21$. (c) The same as (a) but for SS interatomic interactions.

configurations of atoms. In that way we eliminate special features resulting from a particular configuration while simultaneously accounting roughly for 'thermal fluctuations' in atomic positions.

Results were obtained for two internal densities $\overline{\rho}\sigma^2 \simeq 0.13, 0.21$ at a fixed temperature of $k_B T/\epsilon = 1$. Plots of $\mathcal{W}_1(R)$ in figure 5 indicate that in general $\mathcal{W}_1(R)$ is strongly repulsive for short com separations ($R \to 0$). This short-range repulsion is stronger for glassy discs at the higher mean (internal) density, as one can verify by comparing plots in figures 5(a) and (b). Again the length scale of the short-range repulsion is determined by the length scale σ of the underlying interatomic (LJ) potential $\varphi(r)$. Therefore it is not surprising that the higher the density of the glassy discs, the larger the short-range repulsion between them.

However, unlike in the cases considered in section 3.1 a long-range repulsive part of $\mathcal{W}_1(R)$ follows the short-range repulsive branch as R increases beyond the LJ (SS) diameter. More precisely, the range over which $\mathcal{W}_1(R)$ decays to zero is now given by the diameter of the discs themselves (that is, $2r_s = 12\sigma$) rather than by the diameter of the constituent atoms. The results also indicate that the averaged effective potential, apart from the steep repulsion in the range $R \lesssim \sigma$, is rather smooth and follows a simple functional form. In fact, this

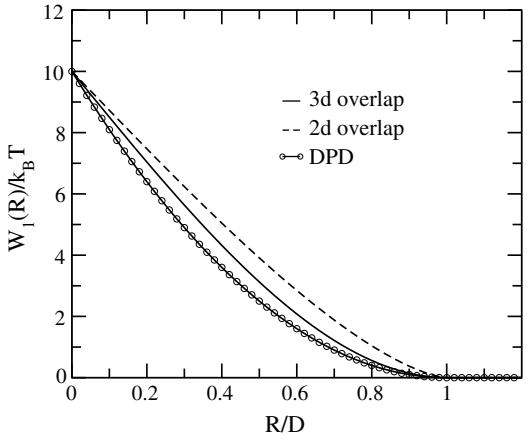

Figure 6. Comparison of the DPD potential (see (3.4)) with the 2D and 3D overlap effective potentials (see (2.54)) for $\beta a_{3D} = \beta a_{2D} = \beta a_{DPD} = 10$ and $D = 2r_0$.

second part of the potential is well represented by the simple 2D overlap potential developed in section 2.5. This can be seen from the fits (based on (2.54), with $r_0 = r_s$) also included in figures 5(a) and (b). The fits have been defined by fixing the constant a_{2D} in (2.54) according to the values of $\mathcal{W}_1(R)$ at separation $R/2r_0 = 3$. It should be noted, however, that this latter choice is essentially arbitrary and other choices would also give satisfactory agreement.

Similar results are obtained for the SS interatomic potential (see (2.4); $\lambda = 0$) as one can see from figure 5(c), where we plot $\mathcal{W}_1(R)$ for this latter potential. The main difference between $\mathcal{W}_1(R)$ for the LJ and SS interatomic potentials concerns the statistical 'noise', which is smaller for the SS effective potential as one can see by comparing plots in figures 5(a) and (c). However, the overlap approximation works again quite nicely for the SS effective potential.

3.4. Properties of 3D 'overlap' fluids

The slow spatial variation of the overlap approximation to the effective potential, in particular the lack of any steep repulsive part, suggests that the overlap potential might also be a suitable candidate for mesoscale computer simulations such as the DPD method [3–6]. The performance of these mesoscale simulation techniques relies heavily on the 'softness' of the underlying potential [23]. For example, many DPD simulations employ an (effective) potential of the form [6, 23]

$$\mathcal{W}_1^{\mathrm{DPD}} = \begin{cases} a_{\mathrm{DPD}}(1 - R/D)^2 & R \leqslant D \\ 0 & R > D \end{cases} \tag{3.4}$$

where D is the diameter of the DPD 'particle'. In figure 6 we compare $\mathcal{W}_1^{\mathrm{DPD}}$ to the overlap potentials in two and three dimensions (see (2.54)), setting the repulsion parameters $a_{3D} = a_{2D} = a_{DPD}$ and the effective diameters $D = 2r_0$. The three potentials have a similar shape. The 3D overlap potential agrees better with the DPD potential than its 2D counterpart employed as a fit function in section 3.3. In the following we thus concentrate on the 3D version, focusing on the question of whether a fluid interacting via the 3D overlap potential has 'soft' properties similar to those of the DPD (and other 'effective') fluids.

In this context the pair correlation function $g(R)$ is of central interest because it enables one to link the structure of the fluid to thermodynamic quantities such as internal energy or

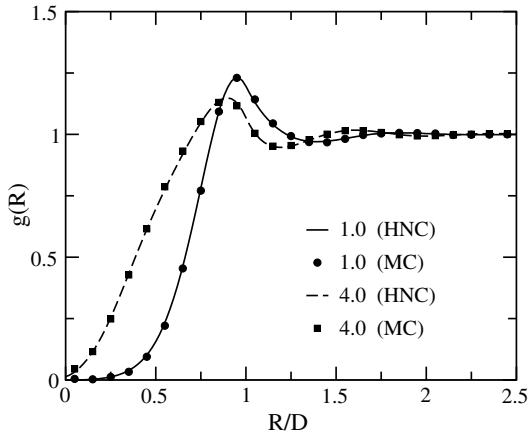

Figure 7. Hypernetted chain (HNC) and Monte Carlo (MC) simulation results for the pair correlation function $g(R)$ for the 3D 'overlap' fluid at reduced densities $\rho D^3 = 1.0$ and 4.0 (reduced repulsion $\beta a_{3D} = 10$).

pressure. We evaluate $g(R)$ both by means of canonical ensemble MC simulations [24] and by means of integral equation theory in the hypernetted chain (HNC) approximation [18]. The latter is given by

$$g(R) = \exp[-\beta \mathcal{W}_1(R) + h(R) - c(R)] \tag{3.5}$$

where $h = g - 1$ and c are the total and direct correlation functions, respectively. These density-dependent functions are linked by the (exact) Ornstein–Zernike (OZ) equation

$$\tilde{h}(k) = \tilde{c}(k) + \rho \tilde{h}(k)\tilde{c}(k) \tag{3.6}$$

where the tilde denotes the Fourier transform. The coupled equations (3.5) and (3.6) can be solved numerically using an iteration procedure (see, e.g., [25]).

Figure 7 compares $g(R)$ obtained by MC simulations and by solution of the integral equations (3.5) and (3.6) for fixed repulsion parameter $\beta a_{3D} = 10$ and two densities. The two methods yield $g(R)$'s that are essentially in quantitative agreement. At both densities the fluid is only weakly structured, as reflected by the absence of higher-order oscillations in $g(R)$ and the rather low first-nearest-neighbour peak around $R/D \approx 1.0$. In addition, as $R \to 0$, $g(R)$ decreases smoothly to a value determined by the repulsion parameter βa_{3D}. Another interesting feature is that $g(R)$ loses rather than gains structure with increasing density. These observations reflect the distinct difference between the overlap potential, on which the $g(R)$'s in figure 7 are based, and an interatomic (e.g., hard-sphere or LJ) potential, for which the structure of $g(R)$ becomes more pronounced with increasing density. The absence of a pronounced shell structure of $g(R)$ for the overlap potential reflects that the number of neighbours around a central particle in the 'overlap' fluid can essentially grow without limit, in contrast to the LJ (or hard-sphere) fluid case, where the coordination number is limited to 12 on average.

The very good agreement between MC and HNC results, which has been reported previously for other ultrasoft potentials [9, 10], is perhaps not surprising. It was established quite some time ago that the HNC closure gives good results for long-range intermolecular potentials [18, 26] such as the Coulomb and dipole–dipole potentials that are in a sense also 'soft' because of their slow decay with increasing R. The HNC closure does not work well, on the other hand, if the interaction potential is dominated by a short-range repulsion, as for the hard- or soft-sphere potentials [18, 26].

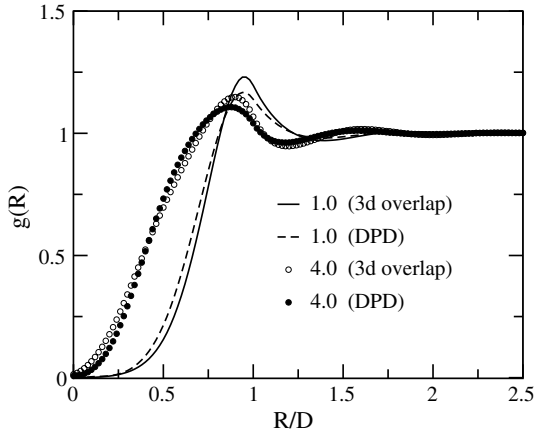

Figure 8. The HNC pair correlation function $g(R)$ for 3D 'overlap' and 'DPD' fluids at two different reduced densities $\rho D^3 = 1.0$ and 4.0 (reduced repulsion $\beta a_{3D} = \beta a_{DPD} = 10$).

The excellent performance of the HNC theory prompted us to employ this approximation to compare properties of the 3D 'overlap' fluid ($\mathcal{W}_1(R)$ given by (2.54)) with those of the 'DPD' fluid ($\mathcal{W}_1(R)$ given by (3.4)). For the two densities $\rho D^3 = 1.0$, 4.0 considered, the resulting $g(R)$'s plotted in figure 8 reveal only slight deviations, the main difference being that the first peak of $g(R)$ for the overlap potential is higher and somewhat more pronounced. This suggests that the 3D overlap potential is slightly less soft than the DPD potential, as indicated already by the potential curves in figure 6.

With the aid of $g(R)$ we can also compute the pressure. Within the HNC approximation (3.5) this can be accomplished in several ways, which permits us to check the internal consistency of our data. We begin by splitting the pressure P into an ideal-gas contribution P^{id} and an excess contribution P^{ex} due to $\mathcal{W}_1(R)$, that is

$$P = P^{id} + P^{ex} \tag{3.7}$$

where

$$P^{ex} = -\frac{2\pi\rho^2}{3}\int_0^\infty \mathrm{d}R\, R^3 \frac{\mathrm{d}\mathcal{W}_1(R)}{\mathrm{d}R}\, g(R) \tag{3.8}$$

follows from the conventional virial route [18]. Another expression for P^{ex}, which is exact within the HNC theory, is derived in the appendix.

Utilizing these two independent expressions we evaluated P^{ex} for a number of densities ρD^3 (and fixed repulsion $\beta a_{3D} = 10$). Results are given in table 1, where we have also included corresponding MC data (based on the virial route [24]). As one can verify, the two routes give nearly identical results for the (reduced) excess pressure. This *internal* consistency is particularly noteworthy in view of the approximate character of the HNC theory. In fact, HNC results for 'ordinary' (e.g., LJ) fluids are typically internally inconsistent [18]. Therefore we conclude that the internal consistency of the data in table 1 is a consequence of the soft character of the overlap potential. A further consequence, which is apparent from the data in table 1, is that the HNC results agree very well with those of the MC simulations.

Finally, it is instructive to examine the ratio P^{ex}/P^{ex}_{MF}, where the mean-field excess pressure P^{ex}_{MF} follows from (3.8) on setting

$$g(R) = 1 \tag{3.9}$$

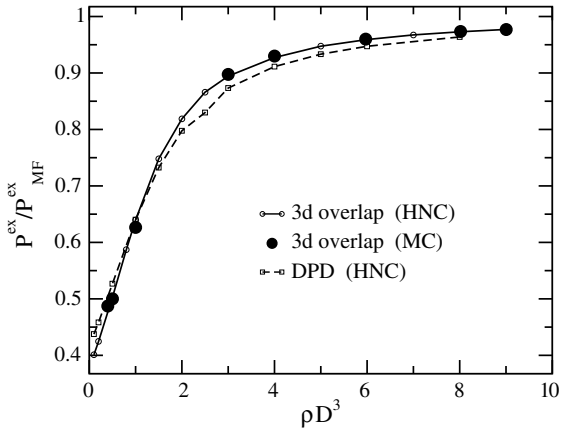

Figure 9. Excess pressure P^{ex} relative to the corresponding mean-field value P^{ex}_{MF} as a function of the reduced density for 3D 'overlap' and 'DPD' fluids.

Table 1. The reduced excess pressure $P^{ex*} = \beta P^{ex} D^3$ for a fluid interacting via the (3D) overlap potential (see (2.54)) for various reduced densities $\rho^* = \rho D^3$ (reduced repulsion $\beta a_{3D} = 10$).

ρ^*	P^{ex*} (see (3.8))	P^{ex*} (see (A.10))	P^{ex*} (MC)
0.5	1.314	1.315	1.308
1.0	1.671	1.674	1.639
2.0	2.140	2.142	—
4.0	2.426	2.428	2.432
6.0	2.507	2.509	2.511
8.0	2.543	2.545	2.546

which expresses the absence of spatial correlations in the mean-field approximation. Substituting (3.9) and the 3D overlap potential (2.54) into (3.8) and performing the integrations, one obtains

$$P^{ex}_{MF} = \frac{\pi}{12} a_{3D} \rho^2 D^3 \tag{3.10}$$

where $D = 2r_0$ is the molecular diameter. Plots of the ratio P^{ex}/P^{ex}_{MF} in figure 9 indicate that the mean-field nature of the 'overlap' fluid increases with increasing ρ (i.e., the ratio tends to unity as ρ gets large). The increasing mean-field character of the fluid is already evident from plots of $g(R)$ in figure 7, where one sees that the fluid loses internal structure as ρ increases. Hence, an (admittedly somewhat crude but useful) approximation such as (3.9) can be expected to improve with increasing ρ. This is in accord with one's intuition [27]. As ρ increases, the number of neighbours with which a central particle in the 'overlap' fluid interacts can rise to very large values—a classic situation where mean-field theory, which becomes exact for infinite-range potentials [28], should work quite well.

4. Summary and conclusions

In this paper we are concerned with the origin of 'softness' of effective potentials acting between supramolecules composed of individual atoms and molecules. The effective potential is directly associated with the free energy of an assembly of several such supramolecules. As a consequence, effective potentials depend *per se* on the thermodynamic state of the system

under investigation. In this sense, effective potentials are not unique, unlike the underlying intermolecular interaction potentials that govern the motion of the atomic constituents of the supramolecules. On the other hand, since the internal degrees of freedom have been 'integrated out', effective potentials typically depend on only a few parameters. This feature is particularly useful in studies of phenomena that occur on scales of length and time large compared to molecular ones. An example is the self-assembly of amphiphilic molecules which takes place on a timescale much larger than that characteristic of motions of internal degrees of freedom of an individual amphiphile [2]. The much larger scales of length and time become accessible [23] because the effective potential is 'soft', that is the effective potential is finite when the supramolecules overlap and vanishes slowly over the range determined by the size of the supramolecule itself rather than that of the constituent atoms.

The simplest non-trivial system that could conceivably provide insight into the origin of 'softness' consists of an atom interacting with a diatomic molecule. The charm of this system is that the effective potential can nearly be calculated in closed form. Our results indicate that even for this simple system the effective potential is 'soft' in the sense that it remains finite as the com distance between the atom and diatomic molecule vanishes (given appropriate values for the bond length of the diatomic molecule). However, the range of the *effective* potential for the atom–diatomic molecule system is determined by the range of the underlying interatomic potentials, that is by the size of the constituent atoms. Attractive tails of the interatomic potentials and vibrations of the diatomic molecule have little impact on the effective potential. However, it is noteworthy that the effective potential becomes 'softer' if vibrations are incorporated.

The range of the effective potential substantially exceeds that of the underlying interatomic potentials only if many-body effects *and* disorder in the internal configurations (i.e., thermal fluctuations) are incorporated. We demonstrate this in two dimensions for a pair of 'glassy discs' consisting of atoms in nearly random configurations. We also show that the origin of 'softness' can be explained roughly in terms of the free energy change occurring as the discs overlap (or as spheres overlap in three dimensions). The overlap approximation contains an undetermined parameter setting the energy scale for the effective potential. This parameter can be determined by fitting the overlap potential to numerical data.

The usefulness of the overlap approximation lies in its simplicity, which is particularly important if one wishes to perform computer simulation studies. The suitability of the overlap approximation is demonstrated in this work for structural ($g(R)$) and 'mechanical' (P^{ex}) properties by comparing results obtained for it with those for a typical potential frequently employed in DPD simulations (see (3.4)). A particularly interesting finding is that the higher the density of the 'overlap' fluid, the less structured the system appears to be. The character of the 'overlap' fluid becomes more and more mean-field-like as the density increases. We thus conclude that the overlap potential falls into the class of 'ultrasoft' potentials, along with the DPD, Gaussian, and other effective potentials [8].

Acknowledgments

We are pleased to acknowledge fruitful discussions with Dr H Bock (North Carolina State University, Raleigh, USA) and Professor Dr C N Likos (Heinrich-Heine Universität, Düsseldorf, Germany). Two of us (SHLK and MS) are also grateful for financial support from the Deutsche Forschungsgemeinschaft via the Emmy-Noether-Programme and grant SCHO 525/7-1. DJD thanks the Alexander von Humboldt Foundation for the generous Research Award that made possible his stay in Germany.

Appendix

Here we derive an alternative expression (to that given in (3.8)) for $P^{\rm ex}$ within the framework of the HNC approximation. Our approach is first to derive explicit expressions for the excess Helmholtz free energy $\mathcal{F}^{\rm ex}$ and excess chemical potential $\mu^{\rm ex}$ and then to substitute these into the Gibbs–Duhem relation

$$-P^{\rm ex}V = \mathcal{F}^{\rm ex} - \mu^{\rm ex}N \tag{A.1}$$

where V is the volume of the system and N is the number of molecules. For this purpose we utilize the following relation [29], exact for pair potentials:

$$\beta\mathcal{F}^{\rm ex} = \frac{\rho^2}{2}\int_0^1 {\rm d}\alpha \int {\rm d}\boldsymbol{R}_1 \int {\rm d}\boldsymbol{R}_2\, \beta g_\alpha(R)\, \frac{\partial \mathcal{W}_1^\alpha(R)}{\partial\alpha}. \tag{A.2}$$

Here α is the 'charging' parameter, which switches the system from non-interacting ($\alpha = 0$) to fully interacting ($\alpha = 1$), and g_α and $\mathcal{W}_1^\alpha$ are the pair correlation function and pair potential corresponding to a given value of the charging parameter. Using the HNC closure relation (3.5), we can express the integrand in (A.2) as

$$\beta g_\alpha(R)\, \frac{\partial \mathcal{W}_1^\alpha(R)}{\partial\alpha} = h_\alpha(R)\, \frac{\partial h_\alpha(R)}{\partial\alpha} - \frac{\partial c_\alpha(R)}{\partial\alpha} - h_\alpha(R)\, \frac{\partial c_\alpha(R)}{\partial\alpha}. \tag{A.3}$$

Inserting (A.3) into (A.2), we can immediately perform the α integrations on the first and second terms. To handle the third term, we invoke Parseval's relation to convert the integral in real space to one in reciprocal space. Explicitly, this integral (I) becomes

$$\begin{aligned} I &= \frac{\rho^2}{2}\int {\rm d}\boldsymbol{R}_1 \int {\rm d}\boldsymbol{R}_2\, h_\alpha(R)\, \frac{\partial c_\alpha(R)}{\partial\alpha} = \frac{V}{(2\pi)^3}\frac{\rho^2}{2}\int {\rm d}\boldsymbol{k}\, \tilde{h}_\alpha(k)\, \frac{\partial \tilde{c}_\alpha(k)}{\partial\alpha} \\ &= -\frac{V}{2\,(2\pi)^3}\int {\rm d}\boldsymbol{k}(1+\rho\tilde{h}_\alpha(k)-1)\frac{\partial}{\partial\alpha}\,(1-\rho\tilde{c}_\alpha(k)) \\ &= -\frac{V}{2\,(2\pi)^3}\int {\rm d}\boldsymbol{k}\left[(1-\rho\tilde{c}_\alpha(k))^{-1}\,\frac{\partial}{\partial\alpha}\,(1-\rho\tilde{c}_\alpha(k)) + \rho\,\frac{\partial}{\partial\alpha}\,\tilde{c}_\alpha(k)\right] \\ &= -\frac{V}{2\,(2\pi)^3}\int {\rm d}\boldsymbol{k}\left[\frac{\partial}{\partial\alpha}\ln(1-\rho\tilde{c}_\alpha(k)) + \rho\,\frac{\partial}{\partial\alpha}\,\tilde{c}_\alpha(k)\right]. \end{aligned} \tag{A.4}$$

The third line of (A.4) follows from the OZ equation (3.6). Equation (A.4) allows us to carry out the α integration on the third term in (A.3). Combining the results gives [30, 31]

$$\frac{\beta\mathcal{F}^{\rm ex}}{V} = \pi\rho^2\int_0^\infty {\rm d}R\, R^2[h(R)]^2 + \frac{1}{4\pi^2}\int_0^\infty {\rm d}k\, k^2[\ln(1-\rho\tilde{c}(k)) + \rho\tilde{c}(k)] - \frac{\rho^2}{2}\tilde{c}(0) \tag{A.5}$$

where the relation $\tilde{c}(0) = \int {\rm d}\boldsymbol{R}\, c(R)$ is used to get the last term.

Now employing the relation $\mu^{\rm ex} = V^{-1}(\partial\mathcal{F}^{\rm ex}/\partial\rho)_{V,T}$, we obtain from (A.5)

$$\begin{aligned} \beta\mu^{\rm ex} = 2\pi\rho\int_0^\infty {\rm d}R\, R^2[h(R)]^2 - \rho\tilde{c}(0) + \rho^2\pi\int_0^\infty {\rm d}R\, R^2\left[2h(R)\,\frac{\partial h(R)}{\partial\rho} - 2\,\frac{\partial c(R)}{\partial\rho}\right] \\ + \frac{1}{4\pi^2}\int_0^\infty {\rm d}k\, k^2\left[(1-\rho\tilde{c}(k))^{-1}\,\frac{\partial}{\partial\rho}\,(-\rho\tilde{c}(k)) + \frac{\partial}{\partial\rho}\,(\rho\tilde{c}(k))\right]. \end{aligned} \tag{A.6}$$

In order to deal with the fourth term of (A.6), we first use the OZ equation (3.6) to replace the factor $(1-\rho\tilde{c}(k))^{-1}$ by $1+\rho\tilde{h}(k)$ and then use Parseval's relation to convert the reciprocal-space integral back to one in the real space. Equation (A.6) can then be recast as

$$\begin{aligned} \beta\mu^{\rm ex} = 2\pi\rho\int_0^\infty {\rm d}R\, R^2\left[[h(R)]^2 - h(R)c(R)\right] - \rho\tilde{c}\,(0) \\ + 2\pi\rho^2\int_0^\infty {\rm d}R\, R^2\left[h(R)\,\frac{\partial h(R)}{\partial\rho} - \frac{\partial c(R)}{\partial\rho} - h(R)\,\frac{\partial c(R)}{\partial\rho}\right]. \end{aligned} \tag{A.7}$$

To handle the terms in (A.7) involving derivatives with respect to ρ, we make use again of the HNC closure (3.5), from which we obtain

$$\frac{\partial g(R)}{\partial \rho} = \frac{\partial h(R)}{\partial \rho} - \frac{\partial c(R)}{\partial \rho} + h(R)\frac{\partial h(R)}{\partial \rho} - h(R)\frac{\partial c(R)}{\partial \rho}. \tag{A.8}$$

From (A.8) it follows immediately that the integrand in the last term on the rhs of (A.7) vanishes. Consequently (A.7) reduces to

$$\beta\mu^{\mathrm{ex}} = 2\pi\rho \int_0^\infty \mathrm{d}R\, R^2 \left[[h(R)]^2 - h(R)c(R)\right] - \rho\tilde{c}\,(0)\,. \tag{A.9}$$

Finally, combining (A.1), (A.5), and (A.9) we obtain the following explicit expression for P^{ex}, which is exact within the HNC approximation:

$$\beta P^{\mathrm{ex}} = \pi\rho^2 \int_0^\infty \mathrm{d}R\, R^2 \left[[h(R)]^2 - 2h(R)c(R)\right] - \frac{1}{4\pi^2}\int_0^\infty \mathrm{d}k\, k^2 \left[\ln\left(1 - \rho\tilde{c}\,(k)\right) + \rho\tilde{c}\,(k)\right] - \frac{\rho^2}{2}\tilde{c}\,(0)\,. \tag{A.10}$$

References

[1] Lehn J M 1995 *Supramolecular Chemistry* (Weinheim: Wiley–VCH)
[2] Shelley J C and Shelley M Y 2002 *Curr. Opin. Colloid Interface Sci.* **5** 101
[3] Hoogerbrugge P J and Koelman J M V A 1992 *Europhys. Lett.* **19** 155
[4] Koelman J M V A and Hoogerbrugge P J 1993 *Europhys. Lett.* **21** 363
[5] Español P and Warren P B 1995 *Europhys. Lett.* **30** 191
[6] Groot R D and Warren P B 1997 *J. Chem. Phys.* **107** 4423
[7] Likos C N 2001 *Phys. Rep.* **348** 267
[8] Likos C N, Hoffmann N, Löwen H and Louis A A 2002 *J. Phys.: Condens. Matter* **14** 7681
[9] Louis A A, Bolhuis P G, Hansen J P and Meijer E J 2000 *Phys. Rev. Lett.* **85** 2522
[10] Louis A A, Bolhuis P G and Hansen J P 2000 *Phys. Rev.* E **62** 7961
[11] Bolhuis P G and Louis A A 2002 *Macromolecules* **35** 1860
[12] Akkermans R L C and Briels W J 2000 *J. Chem. Phys.* **113** 6409
[13] Akkermans R L C and Briels W J 2001 *J. Chem. Phys.* **115** 6210
[14] Likos C N, Löwen H, Watzlawek M, Abbas B, Jucknischke O, Allgaier J and Richter D 1998 *Phys. Rev. Lett.* **80** 4450
[15] Likos C N, Schmidt M, Löwen H, Ballauf M, Pötschke D and Lindner P 2001 *Macromolecules* **34** 2914
[16] Likos C N, Rosenfeldt S, Dingenouts N, Ballauf M, Lindner P, Werner N and Vögtle F 2002 *J. Chem. Phys.* **117** 1869
[17] Dijkstra M, van Roij R and Evans R 1999 *Phys. Rev.* E **59** 5744
[18] Hansen J P and McDonald I R 1986 *Theory of Simple Liquids* 2nd edn (London: Academic)
[19] Press W H, Flannery B P, Teukolsky S A and Vetterling W T 1989 *Numerical Recipes (FORTRAN)* (Cambridge: Cambridge University Press) chapter 4
[20] Gay J G and Berne B J 1981 *J. Chem. Phys.* **74** 3316
[21] Bronstein I N and Semendjajew K A 1981 *Taschenbuch der Mathematik* (Thun, Frankfurt/Main: Deutsch) chapter 2–6
[22] Dautenhahn J and Hall C K 1994 *Macromolecules* **27** 5399
[23] Vattulainen I, Kattunen M, Besold G and Polson J M 2002 *J. Chem. Phys.* **116** 3967
[24] Allen M P and Tildesley D J 1987 *Computer Simulation of Liquids* (London: Academic) chapter 5.5
[25] Klapp S H L and Forstmann F 1997 *J. Chem. Phys.* **106** 9742
[26] Rogers F A and Young D A 1984 *Phys. Rev.* A **30** 999
[27] Archer A J and Evans R 2001 *Phys. Rev.* E **64** 041501
[28] Lebowitz J L and Penrose O 1966 *J. Math. Phys.* **7** 98
[29] Evans R 1979 *Adv. Phys.* **28** 143
[30] Lado F, Foiles S M and Ashcroft N W 1983 *Phys. Rev.* A **28** 2374
[31] Chen X S, Forstmann F and Kasch M 1991 *J. Chem. Phys.* **95** 2832